NASA CR-

AN INVESTIGATION OF RADIATIVE HEAT TRANSFER IN ABSORBING, EMITTING, AND SCATTERING MEDIA

By F. Shahrokhi and P. Wolf

Prepared under Grant No. NGL-43-001-021 by
THE UNIVERSITY OF TENNESSEE SPACE INSTITUTE
Tullahoma, Tenn.

for

NATIONAL AERONAUTICS AND SPACE ADMINISTRATION

For sale by the Clearinghouse for Federal Scientific and Technical Information
Springfield, Virginia 22151 – CFSTI price $3.00

An Investigation of Radiative Heat Transfer in Absorbing, Emitting, and Scattering Media

by

F. Shahrokhi* and P. Wolf+

The University of Tennessee Space Institute

Tullahoma, Tennessee

ABSTRACT

The problem of radiative heat transfer in a nonisothermal medium is considered. The analysis is carried out for the plane, spherical, and cylindrical geometries separated by a cloud of particles. The media are assumed composed of spherical particles of uniform diameter and complex refractive index which emit, absorb, and scatter energy in an anisotropic fashion. The solution of the equation of transfer for the aforementioned media is obtained by finite-difference iteration method.

This study was carried out as part of a research program being performed under NASA Sustaining Grant NGL-43-001-021.

*Associate Professor of Aerospace Engineering

+Graduate Research Assistant

INTRODUCTION

Many heat transfer problems involve radiative heat transfer through media having local inhomogeneities which effect the transmission. Some specific examples of such problems include the following: The luminous particles in solid propellant rocket exhaust; ablation particles in re-entry heat shields; MHD-applications; etc. In each case these inhomogeneities absorb, emit, and scatter energy anisotropically. For a rigorous treatment of problems involving scattering, both the direction and intensity of scattered radiation must be accounted for. However, the problem in general is so complicated that for solutions a compromise has to be made between accuracy and faithfulness to the physical situation. Most of the proposed computational methods are limited to plane, one-dimensional geometries, or in cylindrical geometries to not-fully-participating media. Some analytical methods are built on the possibility to express the scattering distribution functions analytically in very few terms of a series, which limits the applicability particularly in engineering problems. So it is thought that a reasonably simple computational method, which can remove some of those limitations, will be very useful to the engineer who encounters complicated radiation problems; although, in order to be at all successful in an analysis, very far reaching assumptions and simplifications will have to be made.

The radiation energy flow through a medium that absorbs, scatters and re-emits radiation energy, according to a given temperature distribution T(r) within the medium, is a function of the location and the direction into which one measures. It is an integral over the radiation intensity components of all directions in the geometrical space. So the natural approach to the problem is to ask for the intensity field throughout the medium, which is described by the equation of radiation transfer

$$(\vec{s} \cdot \vec{\nabla})\ I_\nu(\vec{r}, \vec{s}) = -\rho\beta_\nu I_\nu(\vec{r}, \vec{s}) + \frac{\rho\sigma_\nu}{4\pi} \cdot \iint_{4\pi} S(\vec{s}, \vec{s}') \cdot I_\nu(\vec{r}, \vec{s}')\ d\omega' + \rho\kappa_\nu I_{bb_\nu}(\vec{r}) \qquad (1)$$

The equation says that the change of the monochromatic radiation intensity I_ν at a position $\vec{r}$, measured from a direction $\vec{s}$, consists of an extinction of energy $-\rho\beta_\nu I_\nu(\vec{r}, \vec{s})$, an addition due to energy scattered from all other directions $\vec{s}'$ into the direction $\vec{s}$ under consideration:

$$\frac{\rho\sigma_\nu}{4\pi} \iint_{4\pi} S(\vec{s}, \vec{s}') \cdot I_\nu(\vec{r}, \vec{s}')\ d\omega'$$

and a re-emission of energy by the medium element at $\vec{r}$ into the direction $\vec{s}$; $\rho\kappa_\nu I_{bb_\nu}(\vec{r})$

where:

I = intensity

ν = frequency

ρ = mass density of the participating medium

β_ν = monochromatic mass extinction coefficient

σ_ν = monochromatic mass scattering coefficient

κ_ν = monochromatic mass absorption = emission coefficient (assuming the validity of Kirchhoff's law)

S = is the normalized scattering distribution function

$d\omega'$ = infinitesimal element of solid angle about the direction $\vec{s}'$ in space

$'$ = incoming ray

$I_{bb_\nu}(\vec{r}) = I_{bb_\nu}(T(\vec{r}))$ = black body emission intensity of the participating medium at the frequency ν, depending on the temperature of the medium.

The boundary conditions to equation (1) result from the fact that intensities radiated from the boundaries into the medium consist of two parts: the energy emitted by the boundary according to its temperature; and the reflected part of the radiation energy impinging from the medium on the boundary.

The non-homogeneous integro-differential equation (1) with several partial differentials in general is with the peculiar boundary conditions, which contain in fact the total solution to the equation, extremely complicated. Solutions have

been worked so far only for various degrees of simplifications.

Since it was intended to try a solution not only in plane, one-dimensional geometries, but also in spherical and cylindrical geometries, as many engineering applications really dictate, the following approach, different from the ones published so far, was envisioned.

ANALYSIS

Apply quadrature approximations to the scattering integral and fulfill equation (1) only at a finite number of directions $\vec{s}_i$, thus making equation (1) into a system of non-homogeneous ordinary or partial differential equations. By using finite-difference representations for the derivatives with respect to the space coordinate and transformations for the derivatives with respect to the direction, make these differential equations into a system of algebraic equations, which, because of its excessive size is not solved by matrix inversion but by iteration.

The approach seems to be suitable for all quasi-one-dimensional problems such as plane, infinitely wide geometries, spherical and cylindrical geometries with full symmetry.

Because of the finite-step procedure, no conditions have to be fulfilled for the property data in their dependence on frequency and temperature, and for the temperature profiles themselves. The problem is solved monochromatically at as many frequencies as seem to be necessary to find the total

radiation energy transfer, over a suitable band model or any other numerical integration over the frequency. The scattering distribution functions may be from scattering theories in analytical form or from measurements in experiments.

PLANE GEOMETRY

The existing methods[1, 2, 3, 4] for the one-dimensional case are thought to be too lengthy and complicated to provide a quick and accurate picture of the radiation flow throughout the medium for a large set of varied materials and configurations to find optimal designs. A numerical iteration of the approximated equation of radiation transfer was tried and found to be a fast means of providing a complete picture of the radiant heat flow characteristics for the plane one-dimensional geometry and axi-symmetric scattering functions.

Partly following earlier analyses[1, 2] the equation of radiation transfer is taken in its one-dimensional form:

$$\cos\theta \cdot \frac{dI_\nu(x,\theta)}{dx} = -\rho\beta_\nu I_\nu(x,\theta) + \frac{\rho\sigma_\nu}{4\pi} \int_{\theta'=0}^{\pi} \int_{\phi'=0}^{2\pi} S(\bar{\alpha}) I_\nu(x,\theta') \sin\theta' \, d\theta' \, d\phi' + \rho\kappa I_{bb_\nu} \tag{2}$$

The inner integral can be computed if the intensity does not depend on ϕ', giving integrated scattering functions as tabulated in earlier works[1, 2].

The outer integral is approximated by a quadrature that allows for the discontinuity of the intensity at the boundaries. The differential is approximated by finite difference quotients. This delivers a set of algebraic equations for the intensities measured into the discrete directions fixed by the quadrature coordinates.

$$I^{+}_{i_{n+1}} = \left(1 - \frac{\rho\beta\Delta x}{\mu_i}\right) I^{+}_{i_n} + \frac{\rho\sigma\Delta x}{2\mu_i} \sum_{j=1}^{k} a_j \left(S_{ij}\, I^{+}_{j_n} + S_{i-j}\, I^{-}_{j_n}\right)$$

$$+ \frac{\rho\kappa\Delta x}{\mu_i} I_{bb_n} \qquad (3)$$

$$I^{-}_{i_{n-1}} = \left(1 - \frac{\rho\beta\Delta x}{\mu_i}\right) I^{-}_{i_n} + \frac{\rho\sigma\Delta x}{2\mu_i} \sum_{j=1}^{k} a_j \left(S_{-ij}\, I^{+}_{j_n} + S_{-i-j}\, I^{-}_{j_n}\right)$$

$$+ \frac{\rho\kappa\Delta x}{\mu_i} I_{bb_n} \qquad (4)$$

$$i = 1, 2, 3 \ldots k$$

where

$\mu = \cos\theta$

σ = mass scattering coefficient

S_{ij} = scattering function for the discrete angles θ_i, θ_j

a = quadrature weight factor

ij = discrete coordinates μ_i, μ_j

n = number of finite difference step

α = relative size of scattering particles

$\bar{\alpha}$ = angle between incoming and scattered ray

K = order of the quadrature = number of coordinates in the range $0 \leq \mu \leq 1.0$

Each intensity value $I_{i_{n+1}}$ at one point x_{n+1} of the space coordinate grid is expressed by all values I_{j_n} of the previous point x_n.

This can be used for an iteration of the system, using the wall emission intensities as starting values for the iteration:

$$I^{+}_{i_1} = I_{bb_1}$$

The monochromatic black body radiation intensity is:

$$I_{bb_\nu}(T) = \frac{2h\nu^3}{c^2} \cdot \frac{1}{\exp(\frac{h\nu}{kT}) - 1} \qquad (5)$$

where

h = Planck's constant

k = Boltzmann constant

c = speed of light in the medium

T = temperature of the medium

The boundary conditions are:

$$I^{+}_{i_1} = (1 - \rho_1) I_{bb_1} + 2\rho_1 \sum_{j=1}^{k} a_j \mu_j I^{-}_{j_1} \quad \text{(Boundary 1)} \qquad (6)$$

$$I^{-}_{i_N} = (1 - \rho_2) I_{bb_N} + 2\rho_2 \sum_{j=1}^{k} a_j \mu_j I^{+}_{j_N} \quad \text{(Boundary 2)} \qquad (7)$$

where

+ = intensities in the range $0 \leq \theta \leq 90°$

- = intensities in the range $90° \leq \theta \leq 180°$

ρ_1, ρ_2 = reflectivity of boundaries 1 and 2

The boundaries are assumed diffusely reflecting and emitting, a condition that can easily be removed. The reflectivities are also assumed not to depend on the angular distribution of the incoming intensities.

The iteration converges fast for optical thicknesses $0.1 \leq \tau_o \leq 30$, which covers sufficiently the range of τ_o about 1.0. The quick convergence allows to work 20 to 30 monochromatic heat flux profiles which can be integrated numerically to give the total heat flux, provided the sets of property values and scattering functions are available and prepared for the case under study. The monochromatic heat flux is:

$$Q_\nu(x_n) = 2\pi \sum_{j=1}^{k} a_j \left(I^{+}_{j_n} - I^{-}_{j_n}\right) \qquad (8)$$

Since the finite step procedure uses about 200 to 300 points along the coordinate between the boundaries, arbitrary temperature profiles in the participating medium can be analyzed accurately.

It was found that low (3, 4) order Gauss quadrature approximations in certain cases cause an appreciable error of the essential wall heat fluxes. The iteration permits to increase the order of quadrature at little cost of computing time and storage space only.

Figure 2 gives the results compared to computations by an earlier analytic method[2], show fair agreement for the frequency range in which the main heat flux is carried.

Deviations in the wall heat fluxes, particularly at the hot walls, appear for the low side band frequencies where little heat flux is carried. It should be noted that the analytical computation was done in third order quadrature, whereas the iteration was already made in fourth order.

Figure 3 shows heat flux profiles and energy source strength profiles* for two representative cases with linear temperature profile and non-gray wall properties. It can be seen that to maintain a linear temperature field in the medium a field of strong energy sources and sinks has to exist in order to fuel or absorb the radiant heat flow. These energy

---

*The energy source strength is the change of the radiation energy flux with the space coordinate.

sources may be created by any non-radiative energy generation or transfer mode. Therefore, only the energy source strength integrated over the frequency has any physical meaning.

In the aforementioned section the method was described for plane, one-dimensional conditions. The governing equation of radiation transfer for these conditions was Equation (2), which was approximated by a system of equations, approximating the integral by a quadrature and the differential $\frac{\partial I_\nu}{\partial x}$ by a simple finite-difference quotient.

This method was extended to scattering media within spherical and cylindrical geometries. It was found to work, however, only within certain limits of the optical thickness.

The problem is posed as follows: Find the monochromatic heat flux distribution in the medium between the walls as presented in the Figure (4).

The spherical and cylindrical cases are assumed completely symmetric, which makes the problems one-dimensional.

SPHERICAL GEOMETRIES

The equation of radiation transfer, describing the intensity field in the region, is now:

$$\mu \frac{\partial I(r, \mu)}{\partial r} + \frac{1 - \mu^2}{r} \frac{\partial I(r, \mu)}{\partial \mu} = -\rho\beta I(r, \mu)$$

$$+ \frac{\rho\sigma}{2} \int_{-1}^{+1} I(r, \mu') \cdot S(\mu, \mu')\, d\mu' + \rho\kappa I_{bb}(r) \qquad (9)$$

With Kirchoff's law, κ, corresponds to the monochromatic mass emission coefficient, $\varepsilon = \kappa$.

The boundary conditions for Equation (9) are for diffusely emitting and reflecting boundaries exactly as in the plane case:

$$I\ (r = R_{in},\ \mu) = (1 - \rho_1) \cdot I_{bb}(r = R_{in},\ \mu) + 2 \cdot \int_{-1}^{0} \mu' \cdot I\ (r = R_{in},\ \mu')\ d\mu' \qquad (10)$$

$$0 \leq \mu \leq 1$$

Subscript 1 refers to the inner boundary.

$$I\ (r = R_{ad},\ \mu) = (1 - \rho_2) \cdot I_{bb}(r = R_{ad},\ \mu) + 2 \cdot \int_{0}^{1} \mu' \cdot I\ (r = R_{ad},\ \mu')\ d\mu' \qquad (11)$$

$$-1 \leq \mu \leq 0$$

Subscript 2 refers to the outer boundary and ρ_2 is the monochromatic reflectivity of this boundary.

To Equation (9) the quadrature approximation of the integral is applied again, generating from (9) a system of differential equations of order 2k, with k = order of the quadrature =

number of coordinates of the quadrature in the half range $0 \leq \mu \leq 1$.

$$\mu_i \frac{\partial I(\mu_i, r)}{\partial r} = -\frac{1 - \mu_i^2}{r} \frac{\partial I}{\partial \mu}\Big)_{\mu_i, r} - \rho\beta I(\mu_i, r) + \frac{\rho\sigma}{2} \sum_{j=1}^{k} a_j$$

$$[S(\mu_i, \mu_j)\, I(\mu_j, r) + S(\mu_i, \mu_{-j})\, I(\mu_{-j}, r)]$$

$$+ \rho\kappa I_{bb}(r) \qquad (12)$$

$$i = 1, 2, 3, \ldots k, -1, -2, -3, \ldots -k.$$

To work the derivatives $\frac{\partial I}{\partial \mu}\Big)_{\mu_i, r}$ a suggestion for a transformation was accepted from S. Chandrasekhar[3].
Assume a function

$$Q_e(\mu) = \frac{2}{2e + 1} [P_{e-1}(\mu) - P_{e+1}(\mu)]$$

$$= \frac{1 - \mu^2}{e(e + 1)} \cdot \frac{dP_e(\mu)}{d\mu} \qquad (13)$$

with $P_e(\mu)$ = Legendre polynomial of order e. The partial derivatives $\partial I/\partial \mu$ can be expressed in the following way: Integrate the integral $\int_{-1}^{1} Q_e \frac{\partial I}{\partial \mu}\, d\mu$ by parts, observing the discontinuity of $I(r, \mu)$ at $r = R_{in}$, $\mu = 0$, and $r = R_{ad}$, $\mu = 0$

The expression

$$\frac{d\, Q_e\ (\mu)}{d\mu} = -P_e(\mu) \tag{14}$$

found by applying recurrence formulations for Legendre polynomials to (13), will be used in the course of the integration:

$$\int_{-1}^{1} Q_e(\mu)\ \frac{\partial I(r,\ \mu)}{\partial \mu}\ d\mu = Q_e(0) \cdot \left[I\ (r,\ \mu = -0)\ -\ I(r,\ \mu = +0)\right] \mp \int_{-1}^{1} I(r,\ \mu)\ \cdot\ P_e(\mu)\ d\mu \tag{15}$$

Within the region $R_{in} < r < R_{ad}$ the intensity $I(r, \mu)$ is continuous for all r, μ and (15) reduces to

$$\int_{-1}^{1} Q_e(\mu)\ \frac{\partial I}{\partial \mu}\ d\mu = \int_{-1}^{1} I(r,\ \mu)\ P_e\ (\mu)\ d\mu \tag{16}$$

Both integrals may be approximated by the same quadrature that was applied to the scattering integral in the main equation (9):

$$\sum_{j=-k}^{+k} a_j\ Q_e\ (\mu_j)\ \frac{\partial I}{\partial \mu}\Big)_{\mu_j, r} \cong \sum_{j=-k}^{+k} a_j\ P_e(\mu_j)\ I\ (\mu_j,\ r) \tag{17}$$

Thus the differentials $\left.\frac{\partial I}{\partial \mu}\right)_{\mu_j, r}$ are expressed by the functional values $I(\mu_j, r)$ at the same coordinates μ.

For all $\left.\frac{\partial I}{\partial \mu}\right)_{\mu_j, r}$ a system of algebraic equations has to be generated by taking for e values of 1, 2, 3 . . . 2k in Equation (17). This system may be written

$$[X] \cdot [I'] = [C] \cdot [I] \tag{18}$$

with the elements chosen for least computational work:

$$I'_j = \left.\frac{\partial I}{\partial \mu}\right)_{\mu_j, r} \cdot \frac{1 - \mu_j^2}{\mu_j} \tag{19}$$

$$j = 1, 2, 3, 4 \ldots k, -1, -2, -3, \ldots -k$$

$$X_{ij} = \frac{a_j \mu_j}{2i(2i + 1)} \cdot \left.\frac{dP_i}{d\mu}\right)_{\mu_j} \tag{20}$$

$$i = 1, 2, 3 \ldots 2k$$

$$C_{ij} = a_j \cdot P_i (\mu_j)$$

$$I_j = I (\mu_j, r)$$

System (18) can be solved immediately to the following extent:

$$[I'] = [X]^{-1} \cdot [C] \cdot [I] = [P_x] \cdot [I] \tag{21}$$

To the differentials $\frac{\partial I(\mu_i, r)}{\partial r}$, a simple finite-difference quotient is applied to the set of equations with the aforementioned boundary conditions and iterated like in the plane case. Close to the boundaries the system (21) has to be modified because of the discontinuity of the intensity as described above. The modification consists of using i = 2, 4, 6, 8 . . . 2k instead of i = 1, 2, 3, 4 . . . 2k, and working the differentials independently in each half-range $-1 \leq \mu \leq 0$ and $0 \leq \mu \leq 1$. This iteration converges in a region of optical thickness $\tau_{o\nu} = \int_{R_{in}}^{R_{ad}} \rho(r) \cdot \beta(r) dr$, as indicated in Figure 5. The range seems not sufficient for lower $\tau_{o\nu}$ about 1.0. The key to improve this range of convergence lies in a more accurate determination of the partial differentials $\frac{\partial I}{\partial \mu}\Big)_{\mu_i, r_n}$.

Figure 6 demonstrates that the numerical error in the finite-step iteration decreases linearly with the step size. The results for this representative example show that the extrapolated finite step error for 200 steps between the boundaries is below 2%. The error increases slightly with optical thickness $\tau_{o\nu}$ with decreasing spherical parameter $r = \frac{R_{in}}{R_{ad}}$, and with decreasing absolute value of the heat flux. In Figure 6 and the following figures only the monochromatic wall heat fluxes, Q_1 at the inner boundary R_{in} and Q_{LL} at the outer boundary R_{ad} are discussed. It seems to be most conclusive to study the

heat transfer in spherical and cylindrical geometries in comparison to the results in plane cases. So the ratios $Q' = \frac{Q \text{ spherical geometry}}{Q \text{ plane geometry}}$ are plotted against the spherical $r = \frac{R_{in}}{R_{ad}}$, which is a similarity parameter. A result $Q'(r)$ is valid for all combinations R_{in} and R_{ad} which have one and the same r.

Since Q_1 and Q_{LL} represent the monochromatic wall heat fluxes at the walls per unit area, the total energy transfer at the inner wall, $Q_1 \cdot 4\pi R_{in}^2$ compared to that at the outer wall, $Q_{LL} \cdot 4\pi R_{ad}^2$ is also demonstrated by a

$$Q_{1 \text{ red.}} = Q_1 \left(\frac{R_{in}}{R_{ad}}\right)^2 = Q_1 \cdot r^2 \qquad (22)$$

The following Figures 7 to 10 indicate that this energy transfer always decreases at both walls, the more spherical the problem becomes. In order to relate the values Q_i' to true magnitudes, each Figure gives the heat flux values in the plane geometry, which is the limit r = 1.0. The heat flux with no medium present, or $\tau_{o\nu} = 0$, is also given as Q_N. This Q_N represents the heat flux per unit area of outer boundary and also the energy transfer through the region to boundary 1, because this energy flow stays constant with no medium interfering. $Q_{N \text{ red}}'$ is $\frac{Q_N(r)}{Q_N(r = 1.0)}$, also referred to outer boundary area.

Figure 7 shall indicate the strong influence of the temperature profile in the medium. Three profiles are compared:

linear $T\left(\frac{X}{L}\right) = 2000 + 2000\ \frac{X}{L}$ (°K)

plus-parabolic $T\left(\frac{X}{L}\right) = 2000 + 2000 \cdot \frac{X}{L}\left(1 + 4 \cdot \left(1 - \frac{X}{L}\right)\right)$ (°K)

minus-parabolic $T\left(\frac{X}{L}\right) = 2000 - 2000 \cdot \frac{X}{L}\left(1 - 4 \cdot \left(1 - \frac{X}{L}\right)\right)$ (°K)

with $X = r_n - R_{in}$, $L = R_{ad} - R_{in}$

Thus the wall temperatures are the same in each case, 2000 °K and 4000 °K, and only the different temperatures within the medium cause the differences in the Q_i'.

Figure 8 shows a comparison of different optical thicknesses $\tau_{o\nu}$ at one temperature profile. Although the curves for low $\tau_{o\nu}$ have to be terminated early because of convergence problems, it can reasonably be extrapolated how $Q'_{1_{red}}$ and Q'_{LL} go to the common limit $Q'_{N_{red}}$ for $\tau_{o\nu} \to 0$.

At the conditions chosen for Figure 9 the effect of the scattering is quite substantial as the mere change of the relative size $\alpha = \frac{d \cdot \pi}{\lambda}$ of the scattering particles from 1.0 to 4.0 shows.

Figure 10 demonstrates the weak influence of the wall reflectivities ρ_1 and ρ_2 on the relative wall heat flux values Q_i' at the optical thickness $\tau_{o\nu} = 5.57$. This should, however,

not lead to the conclusion that the absolute values Q_i are also very close. They differ quite substantially, as the table for r = 1.0 indicates.

CYLINDRICAL GEOMETRIES

The problem is as for spherical geometry, (previous section). With the assumptions stated there, the equation of radiation transfer for the intensity field becomes:

$$\cos\theta \frac{\partial I}{\partial r} + \frac{\sin\phi \cos\phi \cos\theta}{r} \frac{\partial I}{\partial \phi} - \frac{\sin\theta \cos^2\phi}{r} \frac{\partial I}{\partial \theta}$$

$$= -\sigma\beta I + \frac{\rho\sigma}{4\pi} \int_{\theta'=0}^{\pi} \int_{\phi'=0}^{2\pi} S(\theta, \phi, \theta', \phi') \cdot I(r, \theta', \phi')$$

$$\sin\theta' \, d\theta' d\phi' + \rho\kappa I_{bb}(r) \qquad (23)$$

$$I = I(r, \phi, \theta)$$

The intensity I has a symmetry over ϕ for any fixed r and θ:

$$I(r, \theta, \phi) = I(r, \theta, -\phi) = I(r, \theta, \pi-\phi) = I(r, \theta, \pi+\phi) \qquad (24)$$

From this it is concluded and checked by computational results that one may assume an average $\bar{I}(r, \theta)$ over ϕ to be used in the scattering integral in (23), because $I(r, \theta, \phi)$ will not change extremely over ϕ for fixed r, θ.

This allows to reduce the double integral in (23) to a simple integral.

$$\frac{\rho\sigma}{4\pi} \int_{\theta'=o}^{\pi} \int_{\phi'=o}^{2\pi} S(\theta, \phi, \theta', \phi') \cdot I(r, \theta', \phi') \sin \theta' d\theta' d\phi' =$$

$$\frac{\rho\sigma}{2} \int_{-1}^{1} \bar{I}(r, \mu') \cdot S(\mu, \mu') d\mu' \text{ with } \mu = \cos \theta \qquad (25)$$

Introducing the transformations $\cos \theta = \mu$ and $\cos \phi = \zeta$ also in (23) and writing the equation for discrete coordinates μ_i and ζ_e:

$$\frac{\partial I(\mu_i, \zeta_e, r)}{\partial r} = \frac{1}{r} \zeta_e^2 \left(- \frac{1 - \mu_i^2}{\mu_i} \frac{\partial I}{\partial \mu} \right)_{\mu_i, \zeta_e, r} + \frac{1 - \zeta_e^2}{\zeta_e} \cdot \left(\frac{\partial I}{\partial \zeta} \right)_{\zeta_e, \mu_i, r} - \frac{\rho\beta}{\mu_i} I(\mu_i, \zeta_e, r) + \frac{\rho\sigma}{2\mu_i} \sum_{j=1}^{k} a_j [\bar{I}(\mu_j, r) S(\mu_i, \mu_j) + \bar{I}(\mu_{-j}, r) S(\mu_i \mu_{-j})]$$

$$+ \frac{\rho\kappa}{\mu_i} I_{bb}(r) \qquad (26)$$

$i = 1, 2, 3 \ldots k_1, -1, -2, -3 \ldots -k_1$

$e = 1, 2, 3 \ldots k_2$

Generally, the numbers of coordinates μ_i and ζ_e, k_1 and k_2 respectively, on which the equation of transfer shall be fulfilled, could be different. But choosing $k_1 = k_2$ permits to apply the same procedure for the evaluation of the derivatives $\frac{\partial I}{\partial \mu}\Big)_{\mu_i,\ \zeta_e,\ r}$ and $\frac{\partial I}{\partial \zeta}\Big)_{\zeta_e,\ \mu_i,\ r}$. Of course, the kind of quadrature has to be the same. The partial derivative $\frac{\partial I(\mu_i,\zeta_e,r)}{\partial r}$ is replaced again by a simple finite difference quotient, and the system resulting from (26) and from (21), applied to both $\frac{\partial I}{\partial \mu}$ and $\frac{\partial I}{\partial \zeta}$, is iterated as in the plane and the spherical cases.

The Figure 5 indicates the region of convergence for this computation. The limit of convergence compares to that of the spherical case by $[r_{cyl}]_{\text{min. convergence}} > [r_{sphere}]^2_{\text{min. convergence}}$. Figure 11 gives one sample of the relative wall heat fluxes for different temperature profiles. If results of the spherical case are compared with results of the corresponding cylindrical case (which means all parameters are equal, except for $r = \frac{R_{in}}{R_{ad}}$), one finds that they agree within less than about 4%, if the correlation

$$r_{cylindr.} = r^2_{sphere} \tag{27}$$

is used. This property can be considered very helpful, because a problem at hand in cylindrical geometry may be reduced to a spherical problem by just applying (27), and thus the higher

accuracy and the lower computing time (about 1/5) of the spherical case can be utilized.

The remaining task for this numerical analysis is to try to find a way to remove the convergence limit for lower τ_{ov}.

REFERENCES

1. Love, T. J. "An Investigation of Radiant Heat Transfer in Absorbing, Emitting and Scattering Media," ARL Report 63-3, January, 1963.
2. Hsia, H. M. "Radiative Transfer in an Absorbing, Emitting, Anisotropically Scattering, and Non-Isothermal Medium," Ph.D Thesis, University of Oklahoma, 1965.
3. Chandrashekhar, S. "Radiative Transfer," Dover Publications, Inc., New York, 1961.
4. Kourganoff, V. "Basic Methods in Transfer Problems," Dover Publications, Inc., New York, 1963.
5. Sparrow, E. M. and R. O. Cess. "Radiation Heat Transfer," Brooks/Cole Publishing Company, Belmont, California, 1966.
6. Shahrokhi, F. and P. Wolf. "Radiative Heat Transfer in Absorbing, Scattering, and Emitting Medium," NASA CR-1023, April, 1968.
7. Shahrokhi, F. and P. Wolf. "Mie-Scattering Function," NASA CR-1022, April, 1968.
8. Shahrokhi, F. and P. Wolf. Numerical Solutions to the Radiative Heat Transfer Equation for Scattering Medium," AIAA Journal, August, 1968.

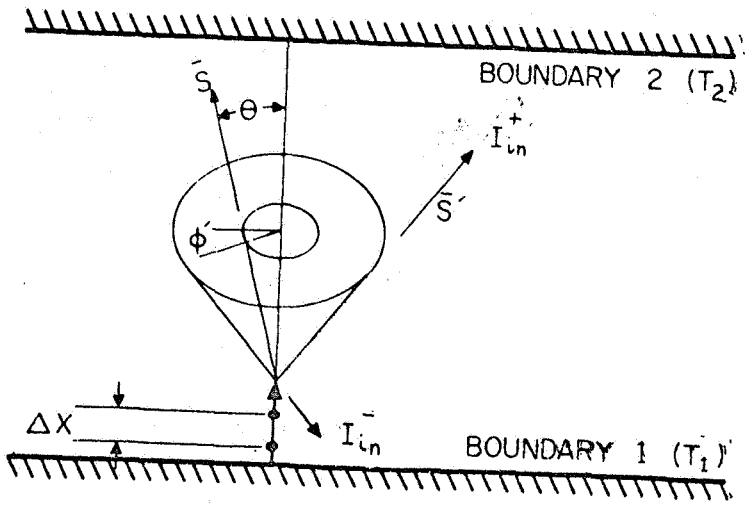

Figure 1. Geometrical model for parallel plates

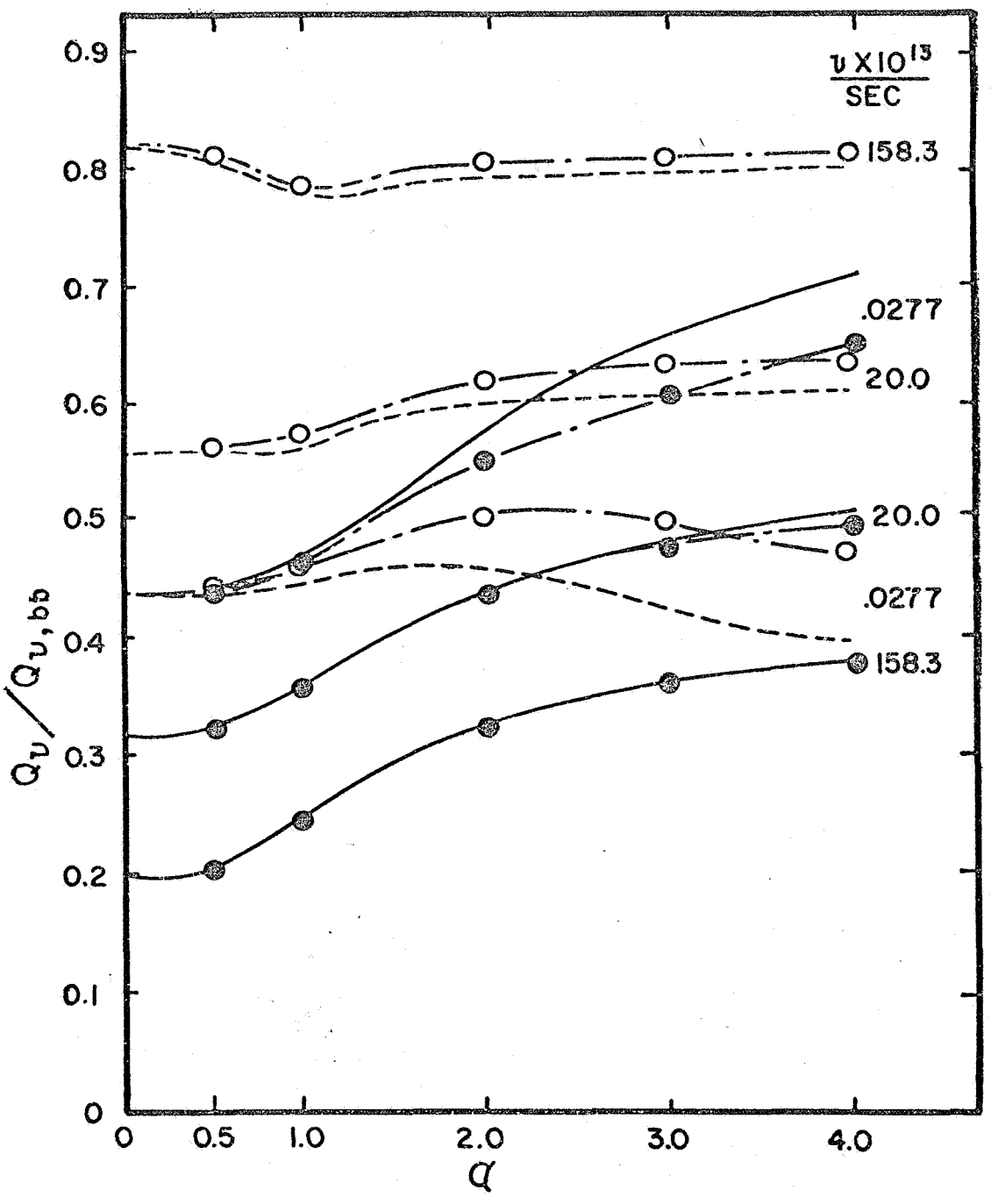

Fig. 2. The effect of radiative transfer at wall 1: $m = 1.25–1.25i$, $\tau_0 = 1.0$, $\rho_1 = \rho_2 = 0.1$, $T_1 = 2000°\text{K}$, $T_2 = 4000°\text{K}$. linear temperature distribution (Hsia)[2]: wall 1; --- wall 2. Present method ● wall 1; ○ wall 2.

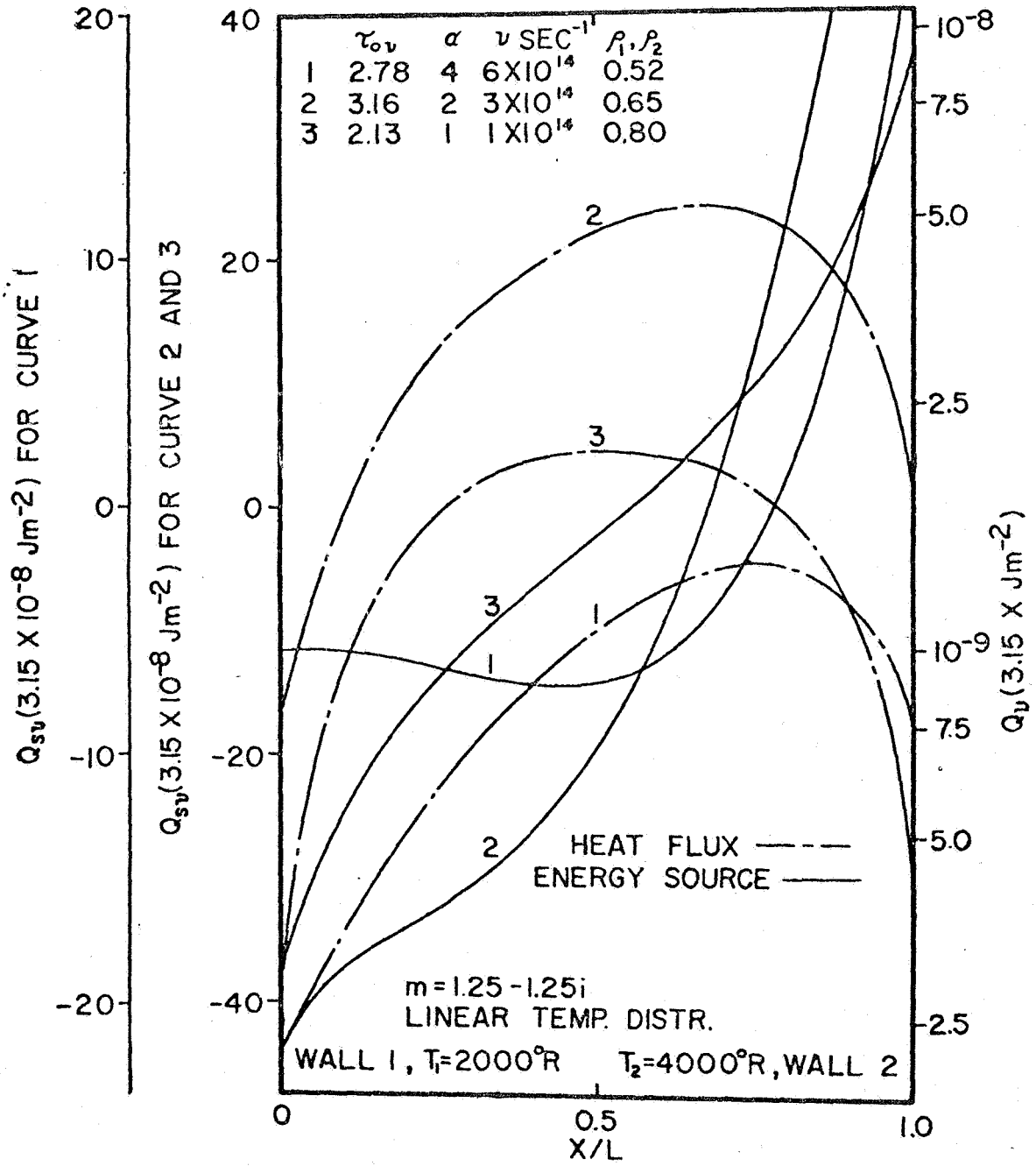

Fig. 3. Monochromatic heat flux and energy source distribution.

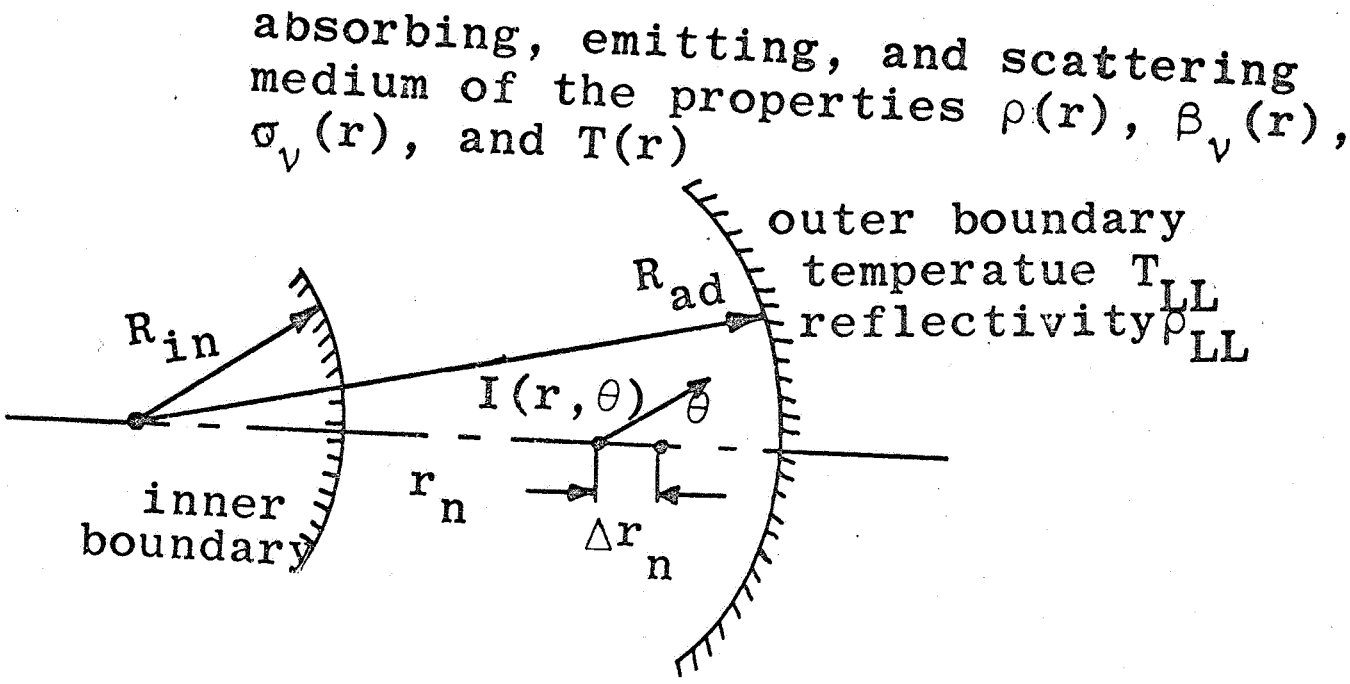

Figure 4. Geometrical model for concentric spheres

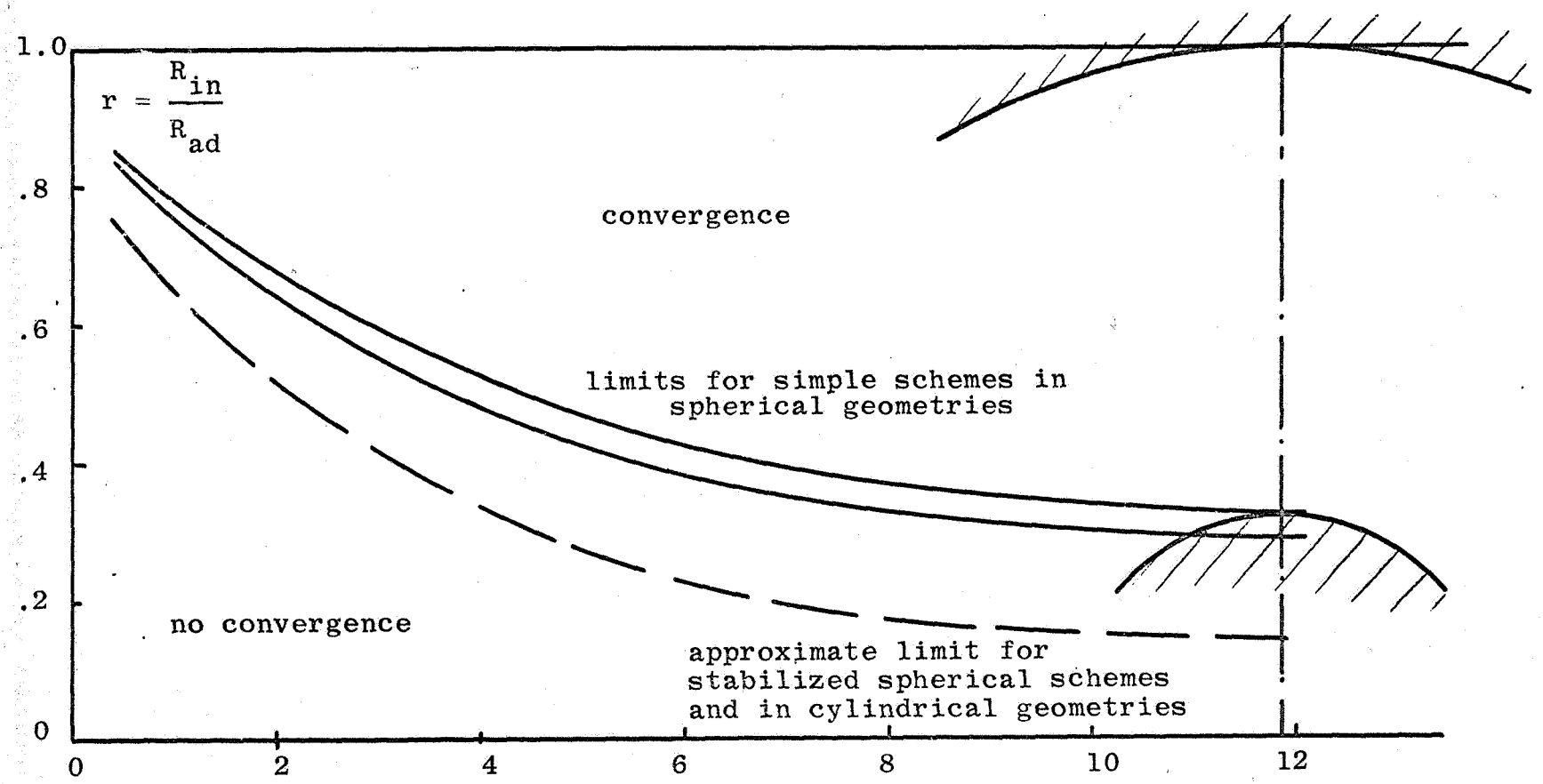

Figure 5. Region of convergence of the iteration in spherical and cylindrical geometries.

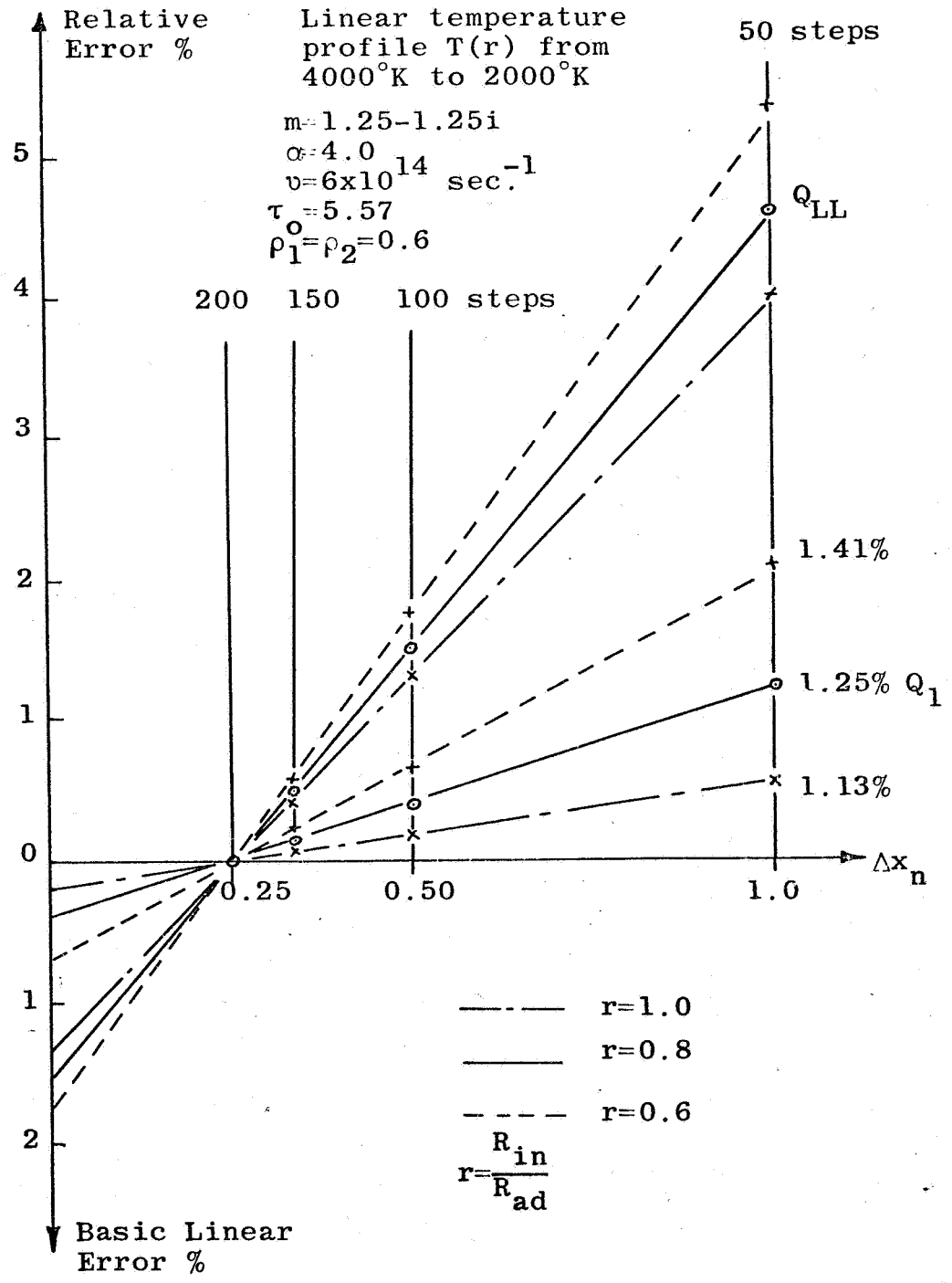

Figure 6. Basic linear error in spherical geometries

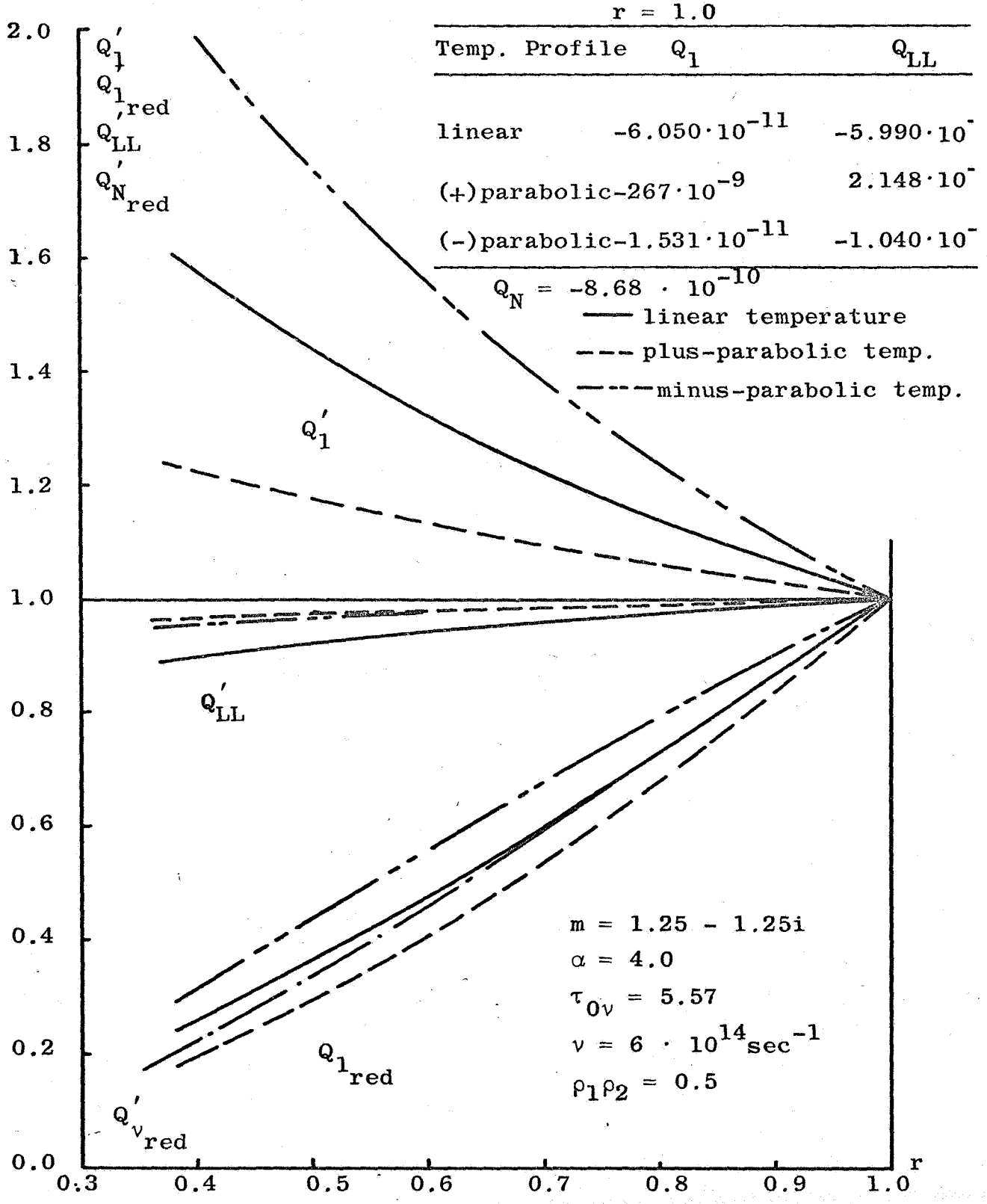

Figure 7. Wall heat flux for different temperature profiles.

r = 1.0

$\tau_{0\nu}$	Q_1	Q_{LL}
1.5	$9.299 \cdot 10^{-10}$	$3.567 \cdot 10^{-10}$
5.58	$5.990 \cdot 10^{-10}$	$6.050 \cdot 10^{-11}$
10.0	$4.217 \cdot 10^{-10}$	$1.372 \cdot 10^{-11}$

$Q_N = 8.68 \cdot 10^{-10}$ Btusechr^{-1} ft^{-2}

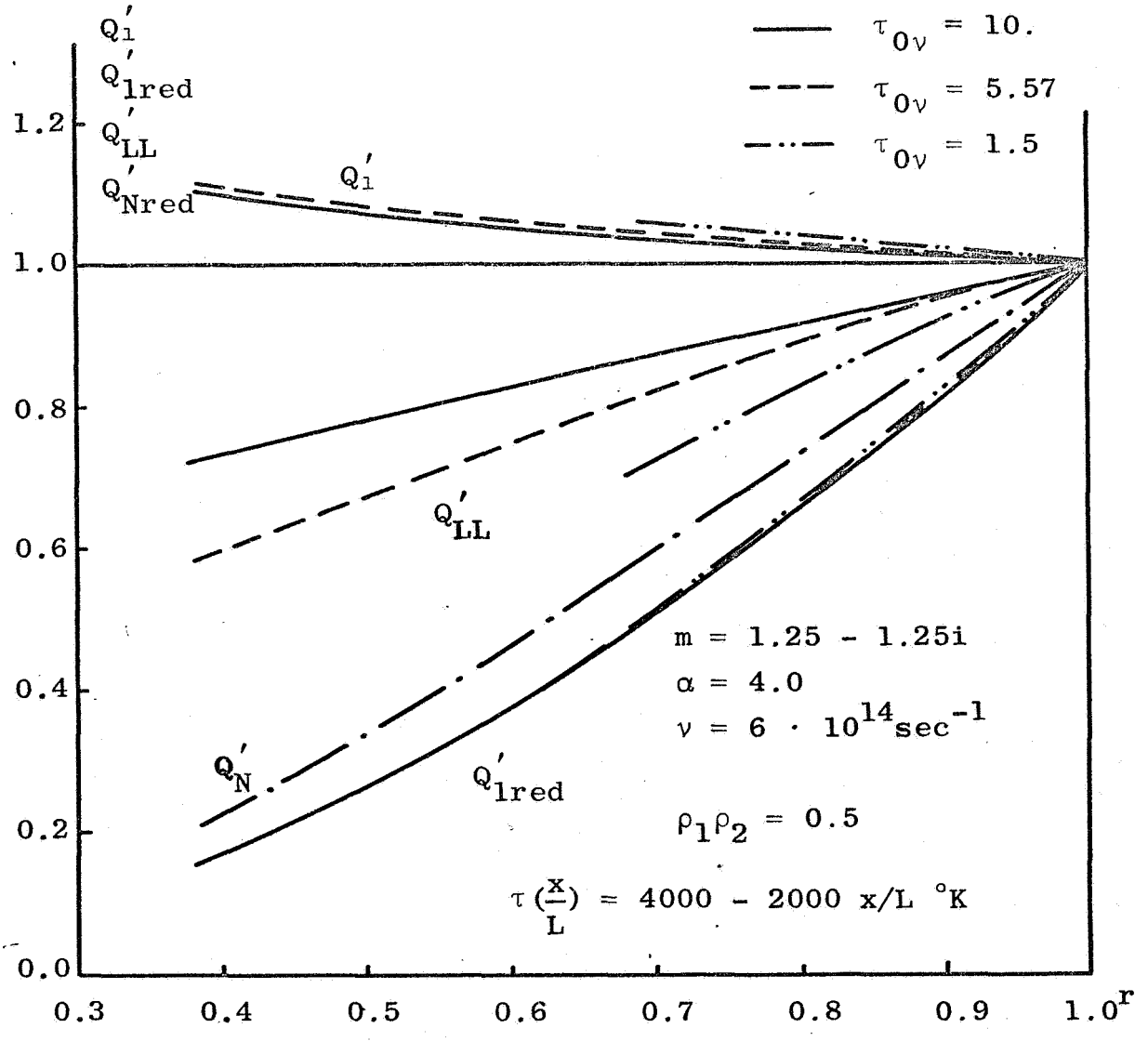

Figure 8. Wall heat flux for different optical thickness $\tau_{0\nu}$

r = 1.0		
α	Q_1	Q_{LL}
1.0	$-4.251 \cdot 10^{-12}$	$-2.992 \cdot 10^{-10}$
4.0	$-1.372 \cdot 10^{-11}$	$-4.217 \cdot 10^{-10}$
1.0	$2.992 \cdot 10^{-10}$	$4.251 \cdot 10^{-12}$
4.0	$4.217 \cdot 10^{-10}$	$1.372 \cdot 10^{-11}$

Btusechr^{-1} ft^{-2}

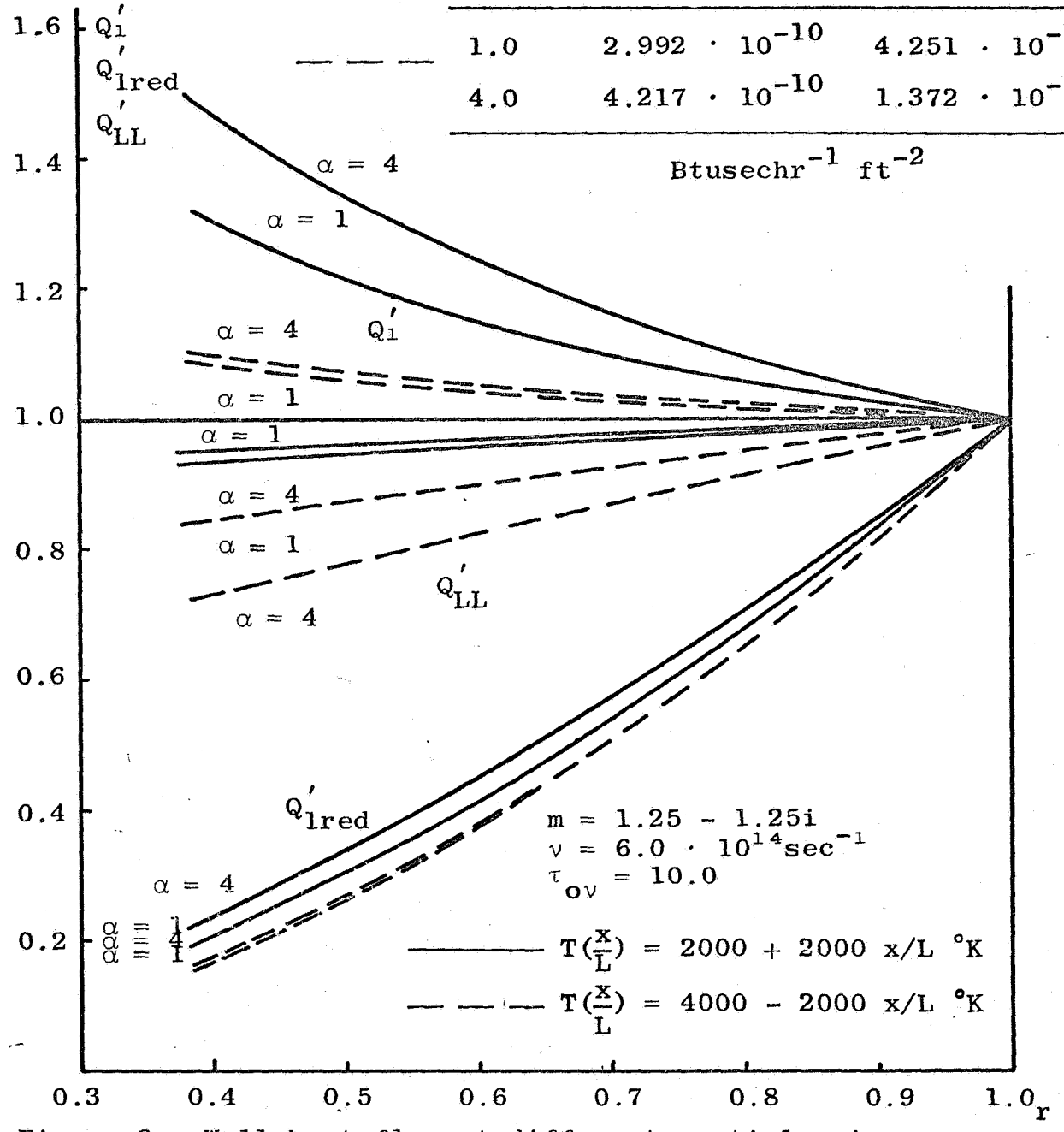

Figure 9. Wall heat flux at different particle size α.

	ρ_1	ρ_2	Q_1	Q_{LL}	Q_N
———	0.5	0.5	$5.990 \cdot 10^{-10}$	$6.050 \cdot 10^{-11}$	$8.68 \cdot 10^{-10}$
– – –	0.9	0.9	$1.273 \cdot 10^{-10}$	$1.106 \cdot 10^{-11}$	$1.37 \cdot 10^{-10}$
—.—	0.1	0.1	$1.063 \cdot 10^{-9}$	$1.149 \cdot 10^{-10}$	$2.13 \cdot 10^{-9}$
o	0.1	0.9	$1.061 \cdot 10^{-9}$	$1.244 \cdot 10^{-11}$	$2.58 \cdot 10^{-10}$
x	0.9	0.1	$1.274 \cdot 10^{-10}$	$1.021 \cdot 10^{-10}$	$2.58 \cdot 10^{-10}$

Btusechr^{-1} ft^{-2}

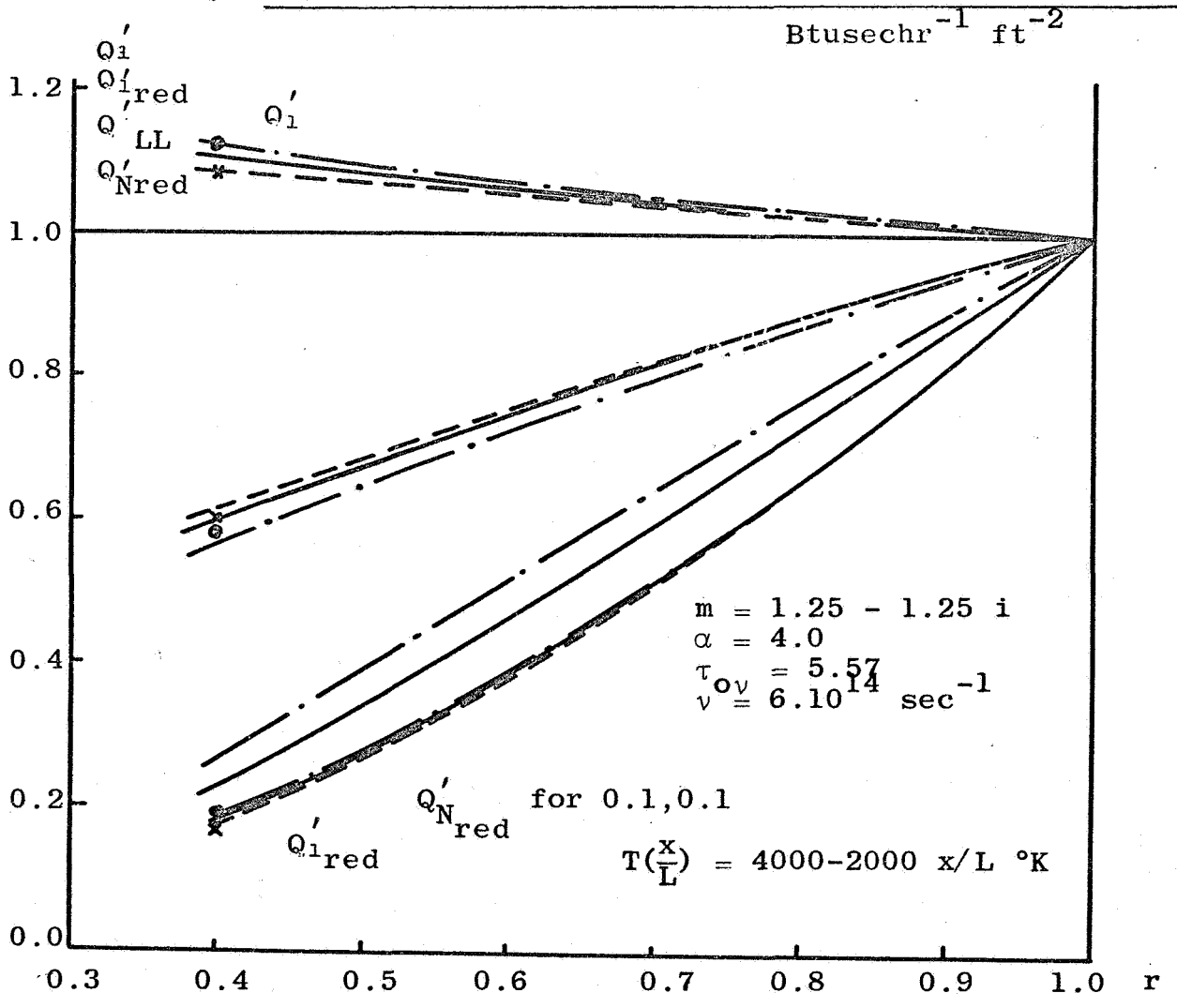

Figure 10. Wall heat flux at different wall reflectivities.

r = 1.0		
Temp. Profile	Q_1'	Q_{LL}'
———	$-6.018 \cdot 10^{-11}$	$-6.016 \cdot 10^{-10}$
- - - - - -	$6.016 \cdot 10^{-10}$	$6.018 \cdot 10^{-11}$
— - —	$1.045 \cdot 10^{-9}$	$1.503 \cdot 10^{-11}$

Btusechr^{-1} ft^{-2}

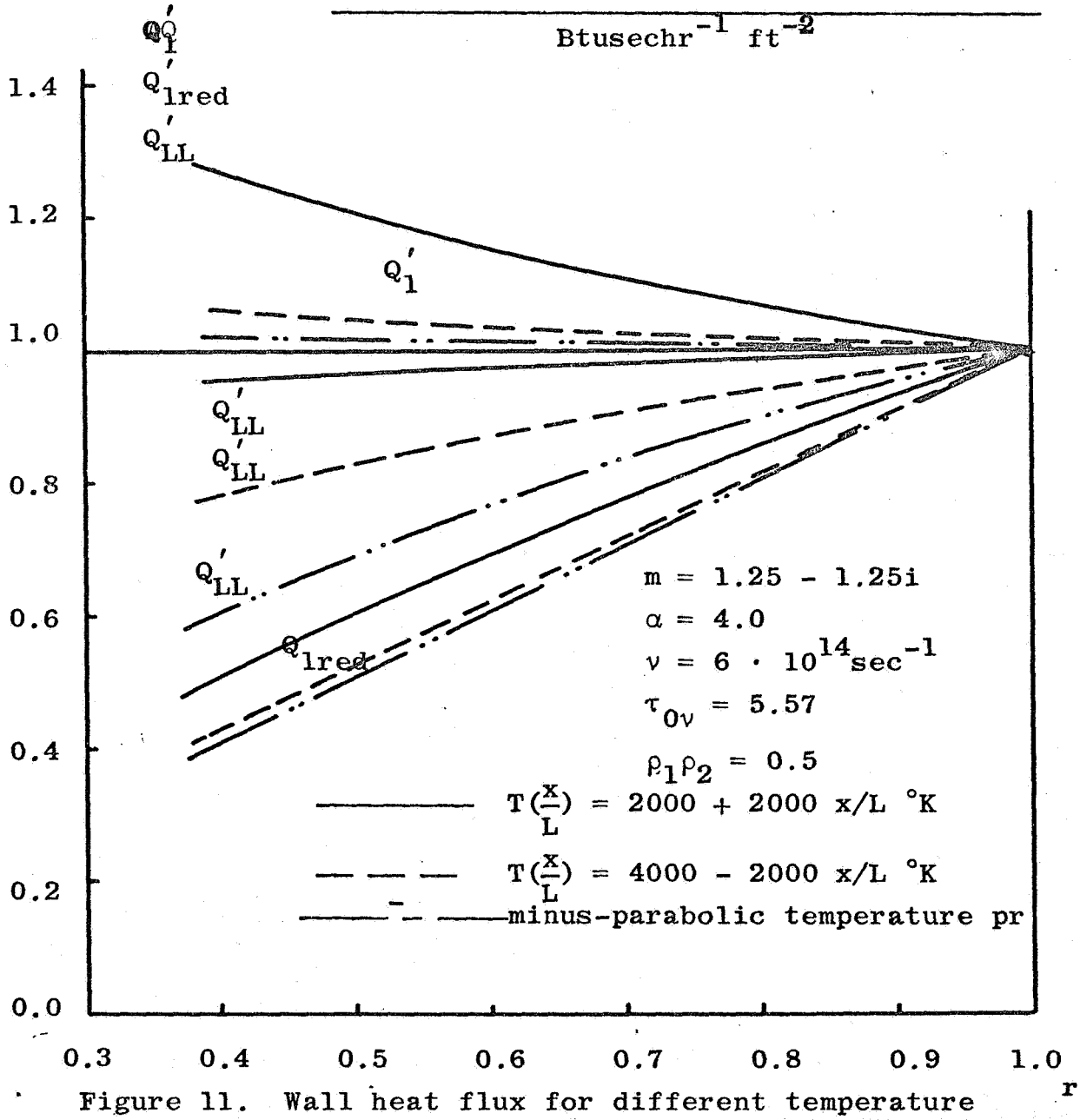

Figure 11. Wall heat flux for different temperature profiles in cylindrical geometry.